JOURNAL OF GUIDANCE, CONTROL, AND DYNAMICS
Vol. 33, No. 2, March–April 2010

Fault-Tolerant Model Predictive Control with Flight-Test Results

Fabio A. de Almeida* and Dirk Leißling†
DLR, German Aerospace Center, 38108 Braunschweig, Germany

DOI: 10.2514/1.46108

This work presents a novel method of fault-tolerant model predictive control where the response of a reference closed-loop model is followed even in the presence of an actuator fault. This architecture is capable of redistributing the control efforts among healthy actuators in a stable manner, respecting their limitations. Also, a constrained guidance system that works in conjunction with the inner-loop fault-tolerant controller is proposed. The guidance law considers the calculated limitations of the inner-loop control system as input constraints in order to smooth the transition between two consecutive navigation legs defined by waypoints. A trajectory-tracking system composed of the constrained guidance and the fault-tolerant model predictive controller is demonstrated through numerical simulations and experimental results on an experimental midsize transport aircraft, showing adequate performance.

Nomenclature

A, B, C	=	continuous-time state-space matrices
A_m	=	reference state-space matrix
c	=	correction vector
d	=	state disturbance vector
d_L	=	lateral deviation, m
E	=	observation matrix
E_a	=	augmented observation matrix
H	=	tracking matrix
I	=	identity matrix
J	=	cost function
K_d, K_g	=	feedback gain matrices
L, L_d, L_x	=	observer gain matrices
N	=	control horizon
n_1	=	perturbation in fan speed, %
O_∞	=	invariant set
$\tilde{O}_\infty$	=	tracking invariant set
P	=	terminal weight matrix
p, q, r	=	aircraft angular rates, deg/s
pla	=	perturbation in power lever angle, deg
Q, W, R	=	weight matrices
Q_d, W_d, R_d	=	discrete weight matrices
Q_m, W_m, R_m	=	implicit model-following weight matrices
Q_{ss}, R_{ss}	=	constrained target calculator weight matrices
r	=	reference vector
T	=	rotation matrix
T_s	=	sampling time, s
t	=	time, s
u_b, v_b, w_b	=	aircraft velocity components in body-fixed axes, m/s
$u_{\max}, u_{\min}$	=	maximum and minimum admissible values of the control vector
V	=	true airspeed, m/s
V_{CAS}	=	calibrated airspeed, kt
w	=	performance output vector
w_m	=	reference model state vector
$\mathbf{X}, \mathbf{U}$	=	admissible state and control sets
X_d, X_r, U_d, U_r	=	unconstrained target calculator matrices
x, u	=	state and control vectors
x_a	=	augmented state vector
x_g	=	guidance state vector
$\hat{x}, \hat{d}$	=	estimated state and disturbance vectors
x_{ss}, u_{ss}	=	state and control vectors at steady state
$\tilde{x}, \tilde{u}$	=	tracking state and control vectors
y	=	observed vector
Z_p	=	pressure altitude, m
z	=	tracking vector
$\Delta\chi_T$	=	angle between navigation legs, deg
δ_a, δ_r	=	aileron and rudder deflections, rad
$\delta_{a_c}, \delta_{r_c}$	=	aileron and rudder commands, rad
λ	=	guidance transition logic gain
Φ, Γ, Γ_d	=	discrete-time state-space matrices
Φ_a, Γ_a	=	augmented discrete-state-space matrices
Φ_g, Γ_g	=	guidance discrete-state-space matrices
ϕ, θ, ψ	=	Euler angles, deg
$\dot{\psi}_c$	=	Yaw rate command, deg/s

Presented as Paper 5621 at the AIAA Guidance, Navigation, and Control Conference, Chicago, IL, 10–13 August 2009; received 24 June 2009; revision received 25 September 2009; accepted for publication 26 October 2009.

*Guest Scientist, Institute of Flight Systems, Lilienthalplatz 7; currently Flight Test Instructor, Grupo Especial de Ensaios em Vôo (GEEV), Campus do Centro Técnico Aeroespacial (CTA), Pça Marechal Eduardo Gomes No. 50, 12228-904 São José dos Campos, São Paolo, Brazil; terrestre.efev@geev.cta.br. Member AIAA.

†Research Scientist, Institute of Flight Systems, Lilienthalplatz 7.

I. Introduction

RECENT decades have been characterized by a significant increase in airspace use. Terminal areas and airways have become more congested, requiring substantial modifications in air traffic regulations, approved charts, and procedures. The high-level environment now presents tighter constraints, in terms of obstacle avoidance and traffic separation. This has resulted in new specifications for aircraft, manned or unmanned, that are intended for operation in such scenarios. The navigation must be more precise and the flight-control system must steer the vehicle over the constrained trajectory, not only during nominal operation but also if a fault should occur in the vehicle.

The primary task of a fault-tolerant controller is to minimize the impact of the fault on the mission objectives. It is desirable to have a vehicle with automatic and self-adjusting capabilities that is able to detect the fault and reorganize the demands in a manner such that the predefined trajectory can continue to be flown. From the point of view of the operator, the aircraft would be capable of following the nominal trajectory without the need of a new sequence of waypoints or airspeeds. Not only could the mission objectives be maintained, but the impact of the trajectory modification on the environment would also be attenuated.

This work considers the problem of tracking a predefined trajectory, as defined by waypoints and target airspeeds, in the presence of actuator faults. Traditionally, fault-tolerant control is achieved through physical redundancy [1,2]. This approach has been used for decades in the aviation industry with consolidated

knowledge and successful architectures commonly based on triple or quadruple redundancy. With the advent of digital computers and their incorporation into onboard systems, fault-tolerant control based on analytical redundancy has gained more attention. In this approach, the redundancy is provided by the aircraft's model incorporated into the controller. Once the fault is detected, the model is modified accordingly and a new control law is generated. Therefore, fault-tolerant control based on analytical redundancy is a model-based method. Fortunately, the topic of aircraft modeling and identification has already reached a mature stage of development [3], so that proper plant models are available.

The application of model predictive control (MPC) to design fault-tolerant controllers is a current topic of research, because MPC can work directly with several types of actuator faults, as well as variations in the open-loop plant model caused by structural damage. Following the work of Heise and Maciejowski [4], several related papers have been published. Maciejowski and Jones [5] proposed the use of MPC to control a large cargo aircraft after it has suffered severe structural damage and loss of control surfaces. Kale and Chipperfield [6,7] presented various formulations of MPC and apply it to a nonlinear model of a fighter aircraft. Recently, Luo et al. [8,9] presented a MPC-based control allocation algorithm and also introduced the concept of dynamic control allocation, referring to control allocation schemes that consider the dynamic characteristics of the actuator.

Despite research effort, most of the implementations of fault-tolerant MPC make use of different prediction and control horizons, where the discrete-state predicted response extends to M steps ahead, using N control moves, $M \geq N$. This type of approach, commonly named finite-horizon MPC, has no guaranteed closed-loop stability [10]. Moreover, since the early 1990s, the MPC formulation has taken the shape of a linear-quadratic regulator (LQR) [11], which is an optimal control technique very familiar to the aerospace community. This MPC variant has finite control horizon N, but the prediction horizon extends towards infinity. The existence of an infinite horizon provides significant design simplifications.

However, the implementation of an infinite horizon MPC provides new challenges. Tracking a desired reference often requires a two-degree of freedom design (i.e., a feedforward part that calculates the target states and control), followed by a regulation scheme around the calculated target values. The target calculation performs a static inversion of the plant, based on a linear model, which is valid inside a limited range of operation. Moving far from the operating point almost certainly will produce a model-plant mismatch and offset errors will typically occur. Also, stable formulations of infinite horizon MPC must incorporate a terminal set constraint, usually involving an invariant set [12]. In tracking applications, the invariant set changes with the time-varying command reference value and also with the input limitations [13]. The computational cost of calculating such sets is still prohibitive for online applications.

Regardless of the choice of horizon (finite or infinite), dynamic closed-loop behavior can change substantially after either input or output saturation. This problem has been investigated by Maciejowski [14] and a change of the tuning parameters has been proposed, but it appears to be impractical in real aerospace applications. Different tuning parameter sets for various types of faults could solve this problem, but would also certainly reduce the level of automation below that required of a fault-tolerant controller.

Moreover, the vast majority of the proposed fault-tolerant controllers focus on modifying the inner-loop control system, because it is assumed that a human pilot would be capable of dealing with the reduced performance and deteriorated flying qualities of the faulty aircraft. Autonomous vehicles must also present such fault tolerance in the outer loops, modifying the guidance laws or even demanding mission replanning. Fault tolerance in multiple control layers is a current topic of research presenting several related challenges such as online determination of the new flight envelope, constrained guidance with reduced maneuverability, and online mission planning [15–18].

Based on these current open issues of model predictive and fault-tolerant control, this article presents a novel MPC formulation with model-following capabilities. The cost function is modified to penalize the deviation of the aircraft's response from a specified closed-loop model, maintaining the nominal closed-loop eigenstructure, even in the presence of failed actuators. The corresponding controller is capable of redistributing the control effort among the healthy actuators. The controller also incorporates a state and disturbance observer to track a desired reference without offset error. The target state and control vectors are calculated while taking into account both the reference to be tracked and the estimated disturbance value. Simulation results are provided that show adequate reconfigurability of the controller (e.g., demanding asymmetric thrust of a two-engine aircraft only from the moment that a rudder fault occurs).

Also, a new constrained lateral guidance system that considers the limitations of the fault-tolerant MPC autopilot is proposed. The statically admissible commands to the inner-loop are treated as constraints by the guidance system. Waypoint transition logic is defined based on invariant sets, which guarantees (based also on a suitable distribution of the waypoints) that the autopilot will be properly demanded and that any geometric overshoots from the desired trajectory will be avoided. The complete controller, composed of the constrained guidance system and a simplified version of the fault-tolerant autopilot, was tested in-flight on the VFW-614 Advanced Technologies Testing Aircraft System (ATTAS; Fig. 1) in a particular scenario of simulated aileron fault, demonstrating adequate performance.

This paper is organized as follows: first, the proposed fault-tolerant model predictive-control technique is presented. Thereafter, the constrained guidance method is introduced and explained. The simulation results of the fault-tolerant MPC are shown and discussed. Finally, the flight-test results obtained on ATTAS are presented and analyzed.

II. Fault-Tolerant Model-Following Predictive Control

This section presents a new model predictive control technique with model-following capability. The weight matrices of the MPC regulator are selected through the implicit model-following technique [19–21]. This choice ensures that the eigenstructure of the closed-loop system will be kept close (in a least-squares sense) to a specified model even with actuator faults, provided that enough analytical redundancy exists in the system. Also, a linear observer is proposed to provide offset-free tracking of a time-varying reference, which significantly improves the robust performance of the controller.

Figure 2 shows the schematic diagram of the proposed solution. The similarity of control redistribution provided by control allocation schemes and optimal control is explored here, considering the dynamics of the actuators and aircraft together in the controller. The discrete controller (circumvented by the dotted line) has three main functionalities: a target calculation, the MPC optimizer, and a linear observer. It is assumed that a fault detection and isolation (FDI) system provides correct information about the status of the actuators to both target calculation and MPC schemes.

The target calculation system calculates the state and control vectors x_{ss} and u_{ss}, respectively, at the steady state, which are

Fig. 1 ATTAS test vehicle.

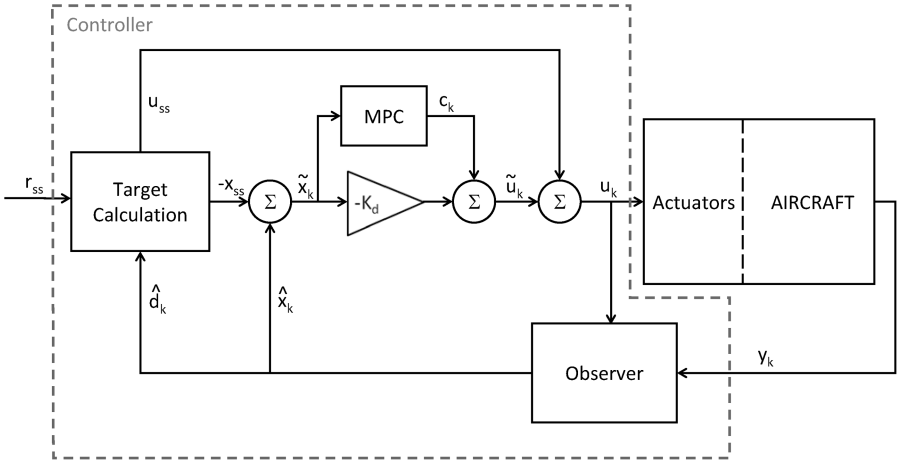

Fig. 2 Fault-tolerant model-following predictive control architecture.

required to give offset-free tracking of the reference r_{ss}. This calculation considers the limitations of the actuators and also those of the aircraft, thus comprising a constrained problem.

The estimated state vector $\hat{x}_k$ is subtracted from x_{ss} to convert the tracking problem to regulation over the desired steady-state condition. In turn, the regulator control law is the sum of two contributions: a linear part with static-linear feedback gain K_d and a nonlinear correction c_k calculated by the MPC system. The MPC is designed such that it only generates corrections if $\tilde{x}_k = \hat{x}_k - x_{ss}$ is such that the linear control part pushes the actuators and/or the aircraft against the limitations. This also means that in the event of an actuator fault, the nonlinear correction c_k redistributes the control effort among the available actuators.

A linear, unconstrained observer is employed in the proposed scheme to provide proper estimates of the disturbance $\hat{d}_k$ and the state $\hat{x}_k$. The estimation of the disturbance is a crucial element to avoid an offset when tracking a desired reference. Here, not only exogenous elements (e.g., turbulence) but also unmodeled dynamics in the actuators and aircraft are considered as disturbances.

A. Constrained Implicit Model-Following Regulator

Let the continuous-time nominal model be defined by

$$\dot{x} = Ax + Bu \qquad w = Cx \tag{1}$$

with state $x \in \mathbb{R}^n$ and control input $u \in \mathbb{R}^m$. Suppose that the performance output w in Eq. (1) is required to follow the transient behavior of the autonomous model:

$$\dot{w}_m = A_m w_m \tag{2}$$

The model matrix A_m has an eigenstructure corresponding to desirable handling qualities of the plant [22,23]. In the case of automatic flight, the model matrix has an eigenstructure that gives a suitable and smooth transient response because, generally, a first-order response or a well-damped second-order response is desired [24].

When the control objective is met, the performance output w will satisfy Eq. (2). Thus one can define an error by

$$e = \dot{w} - A_m w \tag{3}$$

and a cost function by

$$J = \int_0^\infty (e^T Q e + u^T R u)\,\mathrm{d}t \tag{4}$$

Because $\dot{w} = CAx + CBu$, the cost function becomes

$$J = \int_0^\infty (x^T Q_m x + 2x^T W_m u + u^T R_m u)\,\mathrm{d}t \tag{5}$$

where

$$Q_m = (CA - A_m C)^T Q (CA - A_m C) \qquad W_m = (CA - A_m C)^T QCB$$
$$R_m = (B^T C^T QCB + R) \tag{6}$$

Therefore, by appropriately choosing the performance index matrices, it is possible to guarantee implicit model following and thus desirable closed-loop behavior. The continuous dynamical system given by Eq. (1) and the performance index given by Eq. (5) must be discretized in order to be used in an MPC formulation. The discrete form of the dynamical model, assuming that there exists a zero-order hold with sample period T_s at the input [25], is

$$x_{k+1} = \Phi x_k + \Gamma u_k, \qquad k \in \mathbb{N} \tag{7}$$

where

$$\Phi(t) = e^{At} \qquad \Phi = e^{AT_s} \qquad \Gamma(t) = \int_0^t \Phi(t - t')B\,\mathrm{d}t'$$
$$\Gamma = \int_0^{T_s} \Phi(t)B\,\mathrm{d}t \tag{8}$$

The equivalent discrete-step performance index is an infinite sum over the sampled states and inputs

$$J = \sum_{j=0}^{\infty} (x_j^T Q_d x_j + 2x_j^T W_d u_j + u_j^T R_d u_j) \tag{9}$$

that is obtained from Eq. (5) by substituting x by

$$x(t) = \Phi(t)x(0) + \int_t^0 \Phi(t - t')Bu(t')\,\mathrm{d}t' \tag{10}$$

and integrating over one sample period that gives the following weight matrices:

$$Q_d = \int_0^{T_s} \Phi^T(t) Q_m \Phi(t)\,\mathrm{d}t$$
$$W_d = \int_0^{T_s} \Phi^T(t)(Q_m \Gamma(t) + W_m)\,\mathrm{d}t$$
$$R_d = \int_0^{T_s} (R_m + \Gamma^T(t) Q_m \Gamma(t) + W_m^T \Gamma(t) + \Gamma^T(t) W_m)\,\mathrm{d}t \tag{11}$$

Expanding in powers of T_s [26], we have the series expansions

$$Q_d = Q_m T_s + (Q_m A + A^T Q_m) T_s^2/2 + \cdots$$
$$W_d = W_m T_s + (A^T W_m + Q_m B) T_s^2/2 + \cdots$$
$$R_d = R_m T_s + (W_m^T B + B^T W_m) T_s^2/2 + \cdots \tag{12}$$

whereby only the first two terms will be used to approximately determine Q_d, W_d, and R_d.

Considering that both dynamical system and performance index are discretized, we define the discrete constrained optimal control problem. For every sampling time k ($x_0 = x_k$), the following problem must be solved:

$$\min_{\{u_j\}_{j=0}^{\infty}} J(x_0) = \sum_{j=0}^{\infty}(x_j^T Q_d x_j + 2x_j^T W_d u_j + u_j^T R_d u_j)$$

subject to:

$$\begin{aligned} x_{j+1} &= \Phi x_j + \Gamma u_j \\ \{u_j\}_{j=0}^{\infty} &\in \mathbf{U} \\ \{x_j\}_{j=0}^{\infty} &\in \mathbf{X} \end{aligned} \tag{13}$$

The cross-product term $2x_j^T W_d u_j$ in the performance index is necessary to guarantee the desired closed-loop behavior. Moreover, after N sample times, it is desirable to have the state vector inside an invariant set O_∞ for the closed-loop system, where the constraints are no longer active. This terminal constraint will guarantee the stability of the nominal closed-loop system [10]. The adoption of this requirement changes the problem into the following:

$$\min_{\{u_j\}_{j=0}^{N-1}} J(x_0) = x_N^T P x_N + \sum_{j=0}^{N-1}(x_j^T Q_d x_j + 2x_j^T W_d u_j + u_j^T R_d u_j)$$

subject to:

$$\begin{aligned} x_{j+1} &= \Phi x_j + \Gamma u_j \qquad x_N \in O_\infty \\ \{u_j\}_{j=0}^{N-1} &\in \mathbf{U} \\ \{x_j\}_{j=0}^{N-1} &\in \mathbf{X} \end{aligned} \tag{14}$$

where

$$x_N^T P x_N = \sum_{j=N}^{\infty}(x_j^T Q_d x_j + 2x_j^T W_d u_j + u_j^T R_d u_j)$$

is the cost-to-go function and P is the terminal weight given by the solution of the discrete-time Riccati equation:

$$P = Q_d + \Phi^T P \Phi - (\Phi^T P \Gamma + W_d)(\Gamma^T P \Gamma + R_d)^{-1}(\Gamma^T P \Phi + W_d^T) \tag{15}$$

After N sample times, the constraints are inactive and the unconstrained control law $u_j = -K_d x_j$ is valid, where K_d is given by

$$K_d = (\Gamma^T P \Gamma + R_d)^{-1}(\Gamma^T P \Phi + W_d^T) \tag{16}$$

B. Closed-Loop Predictions

To obtain a reconfigurable flight controller, it is desirable to independently design an unconstrained controller plus a supervisory module that gives control corrections in case of an actuator fault. Using MPC, independent design of the two components can be directly obtained by using of closed-loop predictions [27]. The key to this approach is to modify the control law using the following formulation:

$$u_j = \begin{cases} -K_d x_j + c_j, & j = 0, \ldots, N-1 \\ -K_d x_j, & j = N, \ldots, \infty \end{cases} \tag{17}$$

where $c_j \in \mathbf{R}^{Nm}$. Hence, optimization over $\{u_j\}_{j=0}^{N-1}$ can be replaced by optimization over the stacked correction vector $\{c_j\}_{j=0}^{N-1}$. It is clear that, if $x_0 \in O_\infty$, then the unconstrained control law does not violate the constraints and thus $\{c_j\}_{j=0}^{N-1} = 0$. Otherwise, corrections are provided to maintain the state and control vectors inside the admissible sets $\mathbf{U}$ and $\mathbf{X}$.

Thus, the constrained optimal control problem to be solved is given by

$$\min_{\{c_j\}_{j=0}^{N-1}} J(x_0) = x_N^T P x_N + \sum_{j=0}^{N-1}(x_j^T Q_d x_j + 2x_j^T W_d u_j + u_j^T R_d u_j)$$

subject to:

$$\begin{aligned} x_{j+1} &= (\Phi - \Gamma K_d)x_j + \Gamma c_j \qquad x_N \in O_\infty \\ u_j &= -K_d x_j + c_j, \qquad j = 0, \ldots, N-1 \\ \{u_j\}_{j=0}^{N-1} &\in \mathbf{U} \\ \{x_j\}_{j=0}^{N-1} &\in \mathbf{X} \end{aligned} \tag{18}$$

where P and K_d are given by Eqs. (15) and (16), respectively. The solution of the problem expressed by Eq. (18) is made possible by predicting the state vector from the current discrete time until N moves ahead. These prediction equations, as well as the constraint formulation and the conversion of the cost function into a quadratic programming problem can be found in the literature on MPC [28].

C. Reference Tracking

The control problem established in the last section corresponds to regulating the state vector to the origin, given $x_0 = x_k$. Converting this to a tracking control problem is done simply by translating the origin of the state and control vectors to the desired state and control reference values x_{ss} and u_{ss} [29]. Defining $\tilde{x}_j = x_j - x_{ss}$ and $\tilde{u}_j = u_j - u_{ss}$, the regulator problem is converted to a tracker replacing x and u by $\tilde{x}$ and $\tilde{u}$, respectively. The translation also applies to the initial state x_0, admissible sets $\mathbf{U}$, $\mathbf{X}$, and the invariant set O_∞.

This translation technique lacks robustness against a plant-model mismatch. The calculation of x_{ss} and u_{ss} requires the exact knowledge of the state-space model. Thus, the simple change of an operation point or an unknown disturbance acting on the plant can lead to an offset in the reference tracking. Traditional methods for LQR-style state-feedback controllers suggest the addition of the integral of tracking error as an additional state variable [30] to achieve offset-free performance. However, these methods suffer from windup effects as the control reaches saturation.

In recent years, interest in designing offset-free controllers that do not use an integral of tracking error has significantly increased. Using internal model principle [31], one can prove that, if the plant is augmented with as many disturbance states as there are measured variables, then there will be no offset. Recent works [32,33] have explored this principle to choose proper disturbance models and thus design linear, unconstrained state-space observers.

Using the internal model principle, it is also possible to choose disturbance models and design observers augmenting the plant with as many states as there are controlled variables. The advantage of this approach is the reduction of controller complexity because, in most cases, the number of controlled variables is less than the number of measured (observed) variables. This different approach was recently introduced [13,34] and is applied in the following section.

1. Target Calculation

Reconsider the nominal model defined by Eq. (7), now with a disturbance vector d_k:

$$\begin{aligned} x_{k+1} = \Phi x_k + \Gamma u_k + \Gamma_d d_k \qquad d_{k+1} = d_k \\ y_k = E x_k \qquad z_k = H y_k \end{aligned} \tag{19}$$

where $y_k \in \mathbb{R}^p$ is the vector of observed variables, $z_k \in \mathbb{R}^q$, $m \geq q$ is the vector of controlled variables, and $d_k \in \mathbb{R}^q$ is the vector of disturbances. The motivation of incorporating a disturbance vector is to consider mismatches between the plant and the nominal model, as well as external disturbances acting on the plant. The pair (E, Φ) is assumed to be detectable with E full-row rank. Also, the disturbance vector is assumed to be estimated by a proper observer (to be introduced later).

The disturbance model chosen is a simple constant value. If desired, one can choose different dynamics for the disturbance, as

done in [34]. The disturbance matrix Γ_d must be chosen by the designer and thus introduces a degree of flexibility in the design. Its choice may be motivated by an actual disturbance acting on the system or it may allowed to be free as a design parameter. Because the disturbance is not measured, the choice of the disturbance matrix may present a significant challenge.

Thus, the objective of the tracking system is to asymptotically eliminate the control error given a constant reference signal r_{ss}: that is,

$$z_k \underset{k\to\infty}{\longrightarrow} r_{ss} \tag{20}$$

in the presence of a disturbance d_k. This problem corresponds to finding the new equilibrium point of the plant, which turns into the determination of the steady-state target vectors $x_{ss}(r_{ss}, d_k)$ and $u_{ss}(r_{ss}, d_k)$. In steady state, the following relation holds:

$$\begin{bmatrix} I-\Phi & -\Gamma \\ HE & 0 \end{bmatrix}\begin{bmatrix} x_{ss} \\ u_{ss} \end{bmatrix} = \begin{bmatrix} \Gamma_d \\ 0 \end{bmatrix} d_k + \begin{bmatrix} 0 \\ I \end{bmatrix} r_{ss} \tag{21}$$

Thus a unique solution pair x_{ss} and u_{ss} exists for any r_{ss} and d_k if

$$\operatorname{rank}\begin{bmatrix} I-\Phi & -\Gamma \\ HE & 0 \end{bmatrix} = n+q \tag{22}$$

This condition does not hold if some elements of the state are pure integrals of elements of z_k [35]. Under the condition established by Eq. (22), the solution of Eq. (21) can be expressed as [25]

$$\begin{bmatrix} x_{ss} \\ u_{ss} \end{bmatrix} = \begin{bmatrix} X_d & X_r \\ U_d & U_r \end{bmatrix}\begin{bmatrix} d_k \\ r_{ss} \end{bmatrix} \tag{23}$$

where X_d, X_r, U_d, and U_r are the steady-state gain matrices because they map the reference and estimated disturbance directly into control and state vectors. However, it is often the case that constraints are active in the steady state. In the context of fault-tolerant flight control, this may happen when manipulated actuators jam at a nonzero position or the disturbance d_k is large enough to push states and controls against the constraints. Considering that $m \geq q$, the following constrained target calculation problem is solved as follows [11,33,36]:

$$\min_{x_{ss},u_{ss}} J(r_{ss}, d_k) = (HEx_{ss} - r_{ss})^T Q_{ss}(HEx_{ss} - r_{ss}) + u_{ss}^T R_{ss} u_{ss}$$

subject to:

$$\begin{aligned} &(\Phi - I)x_{ss} + \Gamma u_{ss} + \Gamma_d d_k = 0 \\ &u_{ss} \in \mathbf{U} \\ &x_{ss} \in \mathbf{X} \end{aligned} \tag{24}$$

This also corresponds to a quadratic programming problem. The feasibility is guaranteed by the penalization of the difference between the desired (r_{ss}) and reachable (HEx_{ss}) target. If the constraints are too stringent, the reachable target will approach the desired target in a least-squares sense. The second term of the cost function penalizes the control vector in order to produce a small u_{ss}.

Then, the problem (18) is solved to regulate the state and input vector around x_{ss} and u_{ss} and the constrained control law is calculated:

$$\tilde{u}_k = -K_d\tilde{x}_k + c_k \qquad u_k = -K_d(x_k - x_{ss}) + c_k + u_{ss} \tag{25}$$

where $c_k = c_0$ (i.e., the vector composed of the first m elements of the optimal stacked vector $\{c_j^*\}_{j=0}^{N-1}$).

2. Terminal Set Translation

The translation of the origin to the values of x_{ss} and u_{ss} also modifies the state and input constraints imposed on the linear system. Not only must the admissible sets $\mathbf{U}$ and $\mathbf{X}$ be modified, but also the terminal invariant set O_∞. The translated terminal set, here denoted by $\tilde{O}_\infty$, depends on the values of x_{ss} and u_{ss}, which in turn change with r_{ss}. This means that any variation of the demand requires a new invariant set, which would require extensive computational power that is probably not available for real flight control systems. To solve this problem, a parametrization of the invariant set by an extension of the state-space is proposed. Note that, after N steps, the predicted closed-loop system can be expressed as

$$\begin{bmatrix} \tilde{x}_{k+1} \\ u_{ss} \end{bmatrix} = \begin{bmatrix} \Phi - \Gamma K_d & 0 \\ 0 & I \end{bmatrix}\begin{bmatrix} \tilde{x}_k \\ u_{ss} \end{bmatrix} \tag{26}$$

The computation of the invariant set $\tilde{O}_\infty(u_{ss})$ requires the correct formulation of the constraints that are imposed on $\tilde{x}_k$ and u_{ss}. It is clear that the maximum and the minimum values of the control vector can be expressed as a set of linear inequalities in the form

$$-K_d\tilde{x}_j + u_{ss} \leq u_{\max} \qquad K_d\tilde{x}_j - u_{ss} \leq -u_{\min} \tag{27}$$

Therefore, the invariant set $\tilde{O}_\infty(u_{ss})$ of Eq. (26) subject to Eq. (27) must be calculated offline for each selected combination of actuator faults. Then, the dependency of $\tilde{O}_\infty(u_{ss})$ on u_{ss} is eliminated by substitution of the known value of the target control vector. This operation can be performed online because it requires only simple mathematical operations. The resulting set is also invariant, now without depending on u_{ss}.

3. Observer for Offset-Free Tracking

In the previous sections, perfect knowledge of the state and disturbance vectors was assumed. Because the state and disturbance vectors are not directly measured, an observer must be designed and employed. Maeder and Morari [13] propose a linear state/disturbance observer for the augmented plant model obtained from rewriting Eq. (19) as

$$x_{a_{k+1}} = \Phi_a x_{a_k} + \Gamma_a u_k \qquad y_k = E_a x_{a_k} \tag{28}$$

where $x_{a_k} = [\,x_k^T \quad d_k^T\,]^T$ and

$$\Phi_a = \begin{bmatrix} \Phi & \Gamma_d \\ 0 & I \end{bmatrix}, \qquad \Gamma_a = \begin{bmatrix} \Gamma \\ 0 \end{bmatrix}, \qquad E_a = [\,E \quad 0\,] \tag{29}$$

The proposed state/disturbance observer has the form

$$\hat{x}_{a_{k+1}} = \Phi_a\hat{x}_{a_k} + \Gamma_a u_k + L(y_k - E_a\hat{x}_{a_k}) \tag{30}$$

where the estimator gain matrix L is

$$L = \begin{bmatrix} L_x \\ L_d \end{bmatrix} \tag{31}$$

Assuming that the estimated state $\hat{x}_k$ is available at each sampling time, the constrained feedback law stated by Eq. (25) is modified to

$$u_k = -K_d(\hat{x}_k - x_{ss}) + c_k + u_{ss} \tag{32}$$

where x_{ss} and u_{ss} are calculated using Eqs. (23) or (24).

A priori, any technique could be used to find a gain L. However, an offset-free constrained controller is obtained if a certain condition is met, as stated in the following theorem:

Theorem 1. Consider the linear system expressed by Eq. (7) under the control law of Eq. (32). Consider also that the target problem stated by Eq. (23) has a unique solution and the closed-loop system reaches the steady state without active constraints. Furthermore, if

$$\operatorname{null}(L_d) \subseteq \operatorname{null}(H[E(I - \Phi + \Gamma K_d)^{-1}L_x + I]) \tag{33}$$

then $z_{ss} = r_{ss}$.

Proof. When the steady state is reached, Eq. (30) turns into

$$\hat{x}_k = \Phi\hat{x}_k + \Gamma u_k + \Gamma_d\hat{d}_k + L_x(y_k - E\hat{x}_k) \quad L_d(y_k - E\hat{x}_k) = 0 \tag{34}$$

The second part of Eq. (34) also means $(y_k - E\hat{x}_k) \in \operatorname{null}(L_d)$. From the target calculation problem, Eq. (21) follows that

$$x_{ss} = \Phi x_{ss} + \Gamma u_{ss} + \Gamma_d \hat{d}_k \tag{35}$$

Combining Eqs. (32), (34), and (35) yields

$$\hat{x}_k - x_{ss} = (I - \Phi + \Gamma K_d)^{-1} L_x (y_k - E\hat{x}_k) \tag{36}$$

Using Eqs. (21) and (36), the tracking error at the steady state is given by

$$\begin{aligned} Hy_k - r_{ss} &= H(y_k - Ex_{ss}) = H(y_k - E\hat{x}_k + E\hat{x}_k - Ex_{ss}) \\ &= H[E(I - \Phi + \Gamma K_d)^{-1} L_x + I](y_k - E\hat{x}_k) \end{aligned} \tag{37}$$

If the condition Eq. (33) holds, then

$$H[E(I - \Phi + \Gamma K_d)^{-1} L_x + I](y_k - E\hat{x}_k) = 0 \tag{38}$$

which implies $z_{ss} = r_{ss}$.

Based on a similar result, Maeder and Morari [13] propose the following algorithm to construct an observer L:

1) Compute L_x such that $\Phi - L_x E$ is stable and the pair $\bar{H} E_a$ and $\bar{\Phi}$ is detectable, where

$$\bar{H} = H[E(I - \Phi + \Gamma K_d)^{-1} L_x + I] \qquad \bar{\Phi} = \Phi_a - [L_x^T \quad 0]^T E_a \tag{39}$$

2) Compute $\bar{L}_d$ such that $I - \bar{L}_d \bar{H} E(I - \Phi + L_x E)^{-1} \Gamma_d$ is stable.

3) Compute the following matrix:

$$T = \begin{bmatrix} I & -(I - \Phi + L_x E)^{-1} \Gamma_d \\ 0 & I \end{bmatrix} \tag{40}$$

4) Calculate the estimator gain L with

$$L = \begin{bmatrix} L_x \\ 0 \end{bmatrix} + T^{-1} \begin{bmatrix} 0 \\ \bar{L}_d \bar{H} \end{bmatrix} \tag{41}$$

The proposed algorithm allows L_x to be designed first, followed by the disturbance observer. The eigenvalues of $\Phi - L_x E$ (i.e., the state observer dynamics) are not affected by the disturbance observer dynamics.

III. Constrained Lateral Guidance System

The objective of the lateral controller is to regulate the lateral deviation of the aircraft to zero with respect to the active leg of navigation. Therefore, the guidance system that acts in the outer-loop must receive information about the aircraft's present position and then command feasible values to the autopilot.

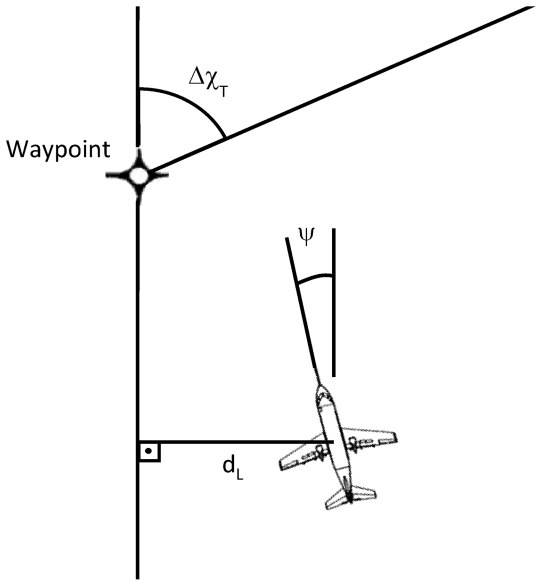

Fig. 3 Elements of the guidance system.

The linearized continuous-time model for lateral navigation (without wind) can be defined by [25]

$$\begin{bmatrix} \dot{\psi} \\ \dot{d}_L \end{bmatrix} = \begin{bmatrix} 0 & 0 \\ V_{\text{trim}} & 0 \end{bmatrix} \begin{bmatrix} \psi \\ d_L \end{bmatrix} + \begin{bmatrix} 1 \\ 0 \end{bmatrix} \dot{\psi}_c \tag{42}$$

where V_{trim} is the trimmed true airspeed (m/s), d_L is the distance (meters) from the desired leg, and ψ is the deviation from the desired heading (rad) (Fig. 3). The lateral deviation is considered positive when the aircraft is to the right of the desired path. The model above, with both poles at 0, comprises a simplification of the closed-loop response of the aircraft, because the closed-loop has an equivalent time response. Also, the presence of steady wind can degrade the closed-loop system performance. Therefore, the guidance control law must be synthesized using control techniques with sufficient robustness against plant-model mismatch and exogenous disturbances.

Because the objective is to fly along a navigation leg, which means $d_L = 0$, the guidance problem can be solved using regulator techniques, such as LQR [37], which has desirable robustness. Thus, at each sampling time instant, an optimal commanded turn rate is calculated based on feedback of lateral deviation and heading deviation. Also, this optimal turn rate command must be calculated with two important constraints. The first arises from the limitations of the reconfigurable autopilot in terms of admissible turn rates, which results in input limitations in the guidance loop. The second limitation is, in fact, a closed-loop specification converted into an output limitation: it is desired to avoid lateral overshoots during the transition between navigation legs. However, this limitation does not necessarily hold along a navigation leg, only during the change from one active leg to another.

In this section, the concept of invariant set is used again for the selection of the optimal point of transition that respects the modeled constraints. Let the discretized closed-loop guidance system be expressed by

$$x_{g_{k+1}} = (\Phi_g - \Gamma_g K_g) x_{g_k} \tag{43}$$

where $x_{g_k} = [\psi_k \quad d_{L_k}]^T$, Φ_g, and Γ_g are the discretized versions of the state-space matrices of Eq. (42) and K_g is a suitable feedback gain. The constraints imposed on Eq. (43) are expressed by the following mathematical inequalities:

$$\begin{aligned} -K_g x_{g_k} \le \dot{\psi}_{c_{\max}} \qquad K_g x_{g_k} \le -\dot{\psi}_{c_{\min}} \qquad d_{L_k} \le 0, \qquad \text{if } \psi_k \ge 0 \\ -d_{L_k} \le 0, \qquad \text{if } \psi_k \le 0 \end{aligned} \tag{44}$$

The first two inequalities are related to the fault-tolerant autopilot capability. The last two express the lateral deviation specification. If the transition causes the heading to change to a positive value (i.e., left turns), only negative values of deviation will be admissible. Conversely, right turns involve only positive admissible values of lateral deviations. Hence, two types of invariant sets will be constructed, considering left or right turns separately. Because $V_{\text{trim}} = 97.8$ m/s and $T_s = 0.05$ in the proposed flight experiment, the maximum invariant set for the system Eq. (43) with $K_g = [0.145 \quad 6.85 \times 10^{-5}]$ and constraints Eq. (44) can be constructed through available numerical techniques [38]. Figure 4 shows the resulting maximal invariant sets for different values of $\dot{\psi}_{c_{\min}} = -\dot{\psi}_{c_{\max}}$.

The invariant sets contract with the decrease of the maximum commanded turn rate. This is in accordance with an important characteristic of maximal invariant sets presented by Gilbert and Tan [39]. It has been demonstrated that the size of such sets is proportional to a scalar value that multiplies the set of constraints. In our case, the maximum invariant set contracts with the same ratio as the maximum commanded turn rate. To maintain integrity, the lateral deviation constraint was modeled with a small value instead of zero in Eq. (44), which also was multiplied by the same factor.

Now it is possible to define a transition logic using the sets shown in Fig. 4. Once the pair formed by the lateral deviation from the next leg and the angle between legs $\Delta\chi_T$ lies inside a maximal set, a transition is possible while respecting the constraints. There are

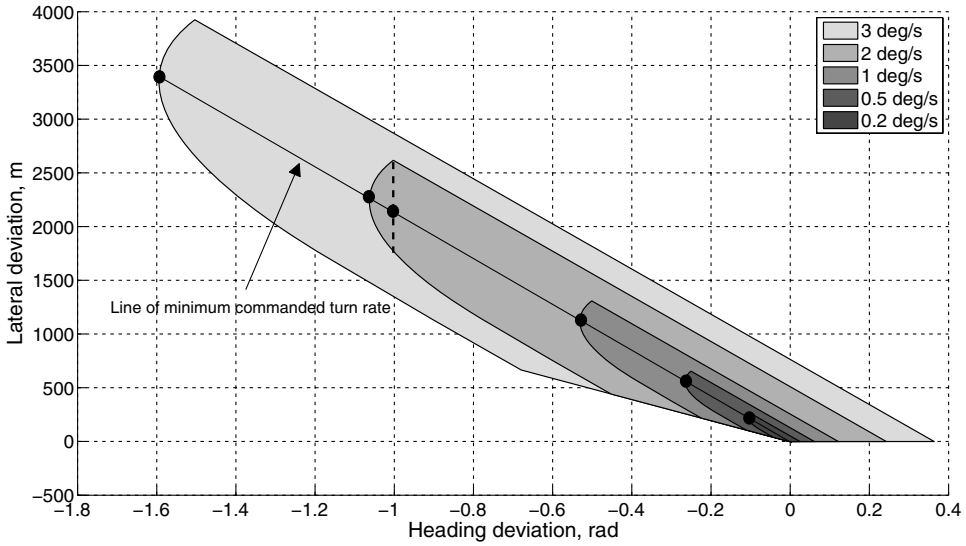

Fig. 4 Constrained guidance maximal invariant sets for different $\dot{\psi}_{c_{\max}}$.

several ways to do the transition; here, two logics will be presented. The first logic minimizes the lateral distance to begin the transition. This is done by considering the initial heading of transition $-\Delta\chi_T$ and then performing a slice of the invariant set at such value. For example, suppose that the autopilot has a maximum admissible command of 2 deg/s of turn rate and the next navigation leg demands $\Delta\chi_T = 57.3$ deg, which corresponds to $\psi_0 = -57.3$ deg. The slice of the related set at this value creates a line segment with extrema 1762–2611 m, as shown in Fig. 4. Thus, the transition can occur when the lateral distance is within these values, and the minimum lateral distance with guaranteed constraint satisfaction is 1.762 km.

The second logic minimizes the commanded turn rate for a given $\Delta\chi_T$. Each invariant set is tangent to a certain value of $\psi_0 = -\Delta\chi_T$. These tangent points, depicted in Fig. 4 with small black circles, are the maximum feasible transition angles for a given limit of commanded turn rate. Also, if a transition begins at such points, the commanded turn rate will be at a minimum (in absolute values). Returning to the same example, the transition with $\Delta\chi_T = 57.3$ deg would start with 2097 m of lateral deviation, demanding no more than 1.88 deg/s.

It is worthy mentioning that transitions starting with lateral distance between 2097 and 2611 m have an S-turn shape; first, a left turn is commanded, followed by a right turn. This behavior is undesirable, but results from the LQR control; therefore, transitions, which use the second logic (minimum commanded turn rate), are preferable.

The property of contraction presented by the maximal invariant set provides a simple way to implement the second logic. The described tangent points are related to each other by the same proportionality constant. Therefore, given $\Delta\chi_T$, the lateral deviation to begin the transition is obtained with a single operation. In the present case, this constant is 2097 m. An additional manipulation is needed to convert the lateral distance to distance of turn anticipation (DTA). Hence, the minimum commanded turn rate transition starts when the distance to the next waypoint is equal to DTA, now expressed by

$$\text{DTA} = 2,097 \text{ m} \frac{\Delta\chi_T}{\sin(\Delta\chi_T)} \tag{45}$$

IV. Simulation Results

The capability of the fault-tolerant MPC described above to redistribute control effort among healthy actuators is demonstrated here. A lateral control case is herein considered because it is desirable to analyze the reconfigurable usage of asymmetrical thrust, but the proposed fault-tolerant technique is also applicable to the design and synthesis of longitudinal controllers.

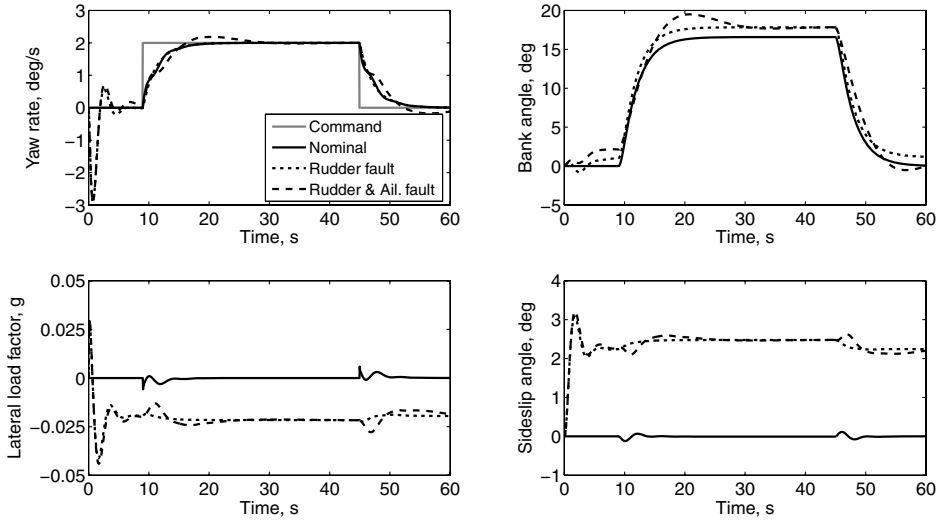

Fig. 5 Evolution of the simulated lateral states.

The MPC tracker makes use of a model description of the open-loop plant to predict the state vector some period of time ahead. The ATTAS linear model considered in this example has been obtained with calibrated airspeed $V_{\mathrm{CAS}} = 145$ kt, pressure altitude of 1000 m, and gear and flaps up. The state vector is

$$x = [\, p \quad r \quad \phi \quad v_b \quad \delta_a \quad \delta_r \quad n_{1_a} \,]^T \tag{46}$$

where p is the roll rate, rad/s), $r \cong \dot{\psi}$ is the yaw rate, rad/s), ϕ is the bank angle, rad, v_b is the lateral velocity component in the body-fixed y axis, m/s, δ_a is the aileron deflection, rad, δ_r is the rudder deflection, rad, and $n_{1_a} = n_{1_l} - n_{1_r}$ is the asymmetric fan speed (i.e., the difference of left and right fan speeds, %). The control vector is $u = [\, \delta_{a_c} \quad \delta_{r_c} \quad \mathrm{pla}_a \,]^T$, which represents the aileron command, rad, rudder command, rad, and asymmetrical power lever angle, deg. The related continuous-time linear model matrices are

$$A = \begin{bmatrix} -1.71 & 0.823 & 0.00440 & -0.0295 & -3.31 & 1.02 & 0.00100 \\ -0.224 & -0.159 & -0.0261 & 0.0209 & -0.241 & -0.975 & 0.00550 \\ 1.00 & 0.102 & 0 & 0 & 0 & 0 & 0 \\ 8.33 & -79.0 & 9.76 & -0.173 & 0 & 2.54 & 0 \\ 0 & 0 & 0 & 0 & -15.8 & 0 & 0 \\ 0 & 0 & 0 & 0 & 0 & -15.8 & 0 \\ 0 & 0 & 0 & 0 & 0 & 0 & -1.15 \end{bmatrix} \tag{47}$$

$$B = \begin{bmatrix} 0 & 0 & 0 \\ 0 & 0 & 0 \\ 0 & 0 & 0 \\ 0 & 0 & 0 \\ 11.5 & 0 & 0 \\ 0 & 12.3 & 0 \\ 0 & 0 & 1.45 \end{bmatrix} \tag{48}$$

The performance output expressed by Eq. (1) is defined by $w = [\, p \quad r \quad \phi \quad v_b \,]^T$, that is required to follow the model given by

$$A_m = \begin{bmatrix} -2.24 & 1.49 & -0.868 & -0.0364 \\ -0.169 & -0.765 & -0.0253 & 0.0257 \\ 1.00 & 0.102 & 0 & 0 \\ 8.11 & -77.4 & 9.60 & -0.186 \end{bmatrix} \tag{49}$$

where A_m has eigenvalues $\{\, -1.70 \quad -0.553 \pm 1.55i \quad -0.386 \,\}$. It is important to emphasize the fact that no actuator dynamical mode is required to follow a model, only the rigid-body aircraft lateral modes. The weight matrices Q and R of Eq. (6) were set as $Q = I$ and

$$R = \begin{bmatrix} 1 \times 10^{-10} & 0 & 0 \\ 0 & 1 \times 10^{-10} & 0 \\ 0 & 0 & 1 \end{bmatrix} \tag{50}$$

where the third diagonal term, which is related to the power lever command, was selected not to give usage of the asymmetric thrust in the nominal (without faults) condition, but rather to provide the proper power lever command allocation in case of fault of the aerodynamic surfaces. The discretization of the dynamical system and the weight matrices is done with $T_s = 0.05$ s, from where the matrices Φ, Γ, Q_d, W_d, and R_d are obtained, as well as the feedback gain:

$$K_d = \begin{bmatrix} -0.417 & 0.0135 & -0.768 & -0.00114 & 1.81 & -0.00612 & -0.00184 \\ 0.268 & -1.83 & 0.182 & 0.0129 & -0.00372 & 1.70 & -0.00233 \\ -0.0191 & -0.377 & -0.0788 & -0.000270 & 0.454 & 0.752 & 0.917 \end{bmatrix} \tag{51}$$

The target calculation problem assumes that the controlled variables are $z = [\, \dot{\psi} \quad n_y \,]^T$ and also that the full state is observed; with respect to Eq. (19), this leads to $E = I$ and

$$H = \begin{bmatrix} 0 & 1 & 0 & 0 & 0 & 0 & 0 \\ 0.0179 & 0.104 & 0 & -0.0176 & 0 & 0.259 & 0 \end{bmatrix} \tag{52}$$

The weights from Eq. (24) were set as $Q_{ss} = I$ and $R_{ss} = 1 \times 10^{-8} I$. The disturbance model was chosen with two variables and the related distribution matrix Γ_d was built taking the first and the third columns of Γ. This arbitrary choice guarantees that the augmented system given by Eq. (29) is detectable. The observer gain L was obtained from the algorithm proposed in Sec. II.C.3, where both L_x and L_d were determined through LQR technique. In the nominal conditions, the set of admissible controls was considered as

$$\begin{gathered} -40^\circ \le \mathrm{pla}_a \le 40^\circ \qquad -60^\circ/sT_s \le \Delta\mathrm{pla}_a \le 60^\circ/sT_s \\ -15^\circ \le \delta_{a_c} \le 15^\circ \qquad -10^\circ \le \delta_{r_c} \le 10^\circ \end{gathered} \tag{53}$$

Figures 5–7 show the simulation results of the nominal condition (no fault) and two fault cases with control horizon $N = 40$, considering a yaw rate command of $2^\circ/\mathrm{s}$ after 9 s. The first fault corresponds to a jammed rudder at deflection 10° from the beginning of the simulation, simulating a scenario where the hydraulic power of the rudder actuator is lost, and then the surface became stuck. The fault is communicated to the controller by changing the rudder constraint to $9.95^\circ \le \delta_{r_c} \le 10.05^\circ$. The second case simulates the same rudder jamming, but also with a 50% loss of aileron effectiveness (structural failure) without being communicated to the MPC prediction model, which continues to calculate the optimal solution based on the nominal state-space model and estimated disturbance vector $\hat{d} = [\, \hat{d}_1 \quad \hat{d}_2 \,]^T$.

The dynamical responses have similar transient shape and zero steady-state errors in the yaw rate, but with a small offset in the lateral load factor. This occurs because the condition of steady state without active constraints, established in Theorem 1, has not been satisfied. However, the small value is still adequate for a passenger aircraft.

Although the aileron fault has not been communicated to the autopilot, it was properly accommodated through the correct estimation of the disturbance vector, as shown in Fig. 6. The elements of the disturbance vector are practically zero, in both nominal and rudder fault scenarios, because there is no plant-model mismatch. The mismatch occurs in the case of rudder and aileron faults, and the estimated elements $\hat{d}_1$ and $\hat{d}_2$ are crucial to avoid steady-state error in yaw rate. Also, the reconfigurability of the proposed fault-tolerant MPC is demonstrated by the usage of asymmetrical thrust. When the actuators are in the nominal conditions, only the aileron and rudder are required. Once the rudder fault is detected and communicated to

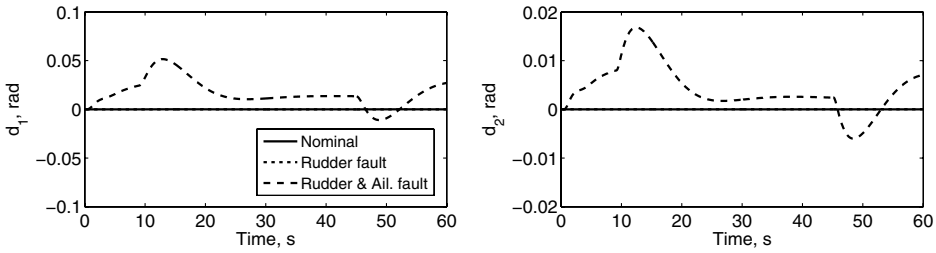

Fig. 6 Evolution of the estimated disturbance vector elements during simulation.

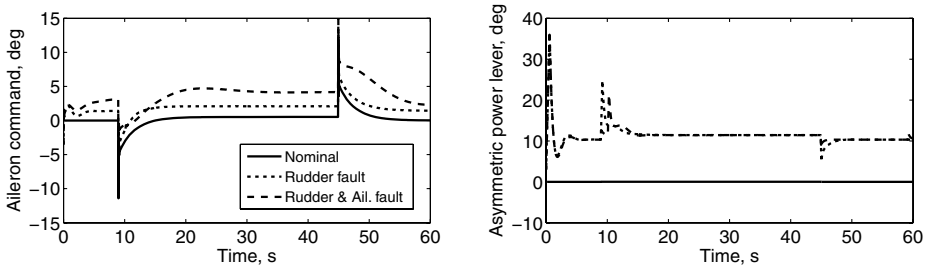

Fig. 7 Evolution of the simulated aileron and asymmetric power lever commands.

the controller, the asymmetrical thrust is commanded not only for the trimmed condition, but also to keep the desired transient response.

V. ATTAS Implementation and Flight-Test Results

The trajectory-tracking controller implemented on ATTAS is presented in Fig. 8. The longitudinal autopilot is commanded by inputs of calibrated airspeed and pressure altitude from the guidance panel in the cockpit. Inside the autopilot, the airspeed controller uses the sum of left and right power lever angles $\text{pla}_t = \text{pla}_l + \text{pla}_r$ as input, and the altitude controller employs the elevator command δ_{e_c} to track and maintain the target flight level and also to provide stability augmentation. Both controllers were designed through single-input/single-output techniques [40].

In the lateral controller the fault-tolerant MPC and the constrained guidance techniques were applied. The outer-loop is demanded by a sequence of waypoints defined by geodetic latitude and longitude. Based on the present position of the aircraft, the lateral distance from the active leg of navigation is calculated and regulated to zero by the guidance system, which considers the maximum statically achievable yaw rate of the MPC autopilot in order to initiate the transition from one active navigation leg to another. Finally, the MPC autopilot manipulates the aileron command δ_{a_c} and the rudder command δ_{r_c} in order to track the yaw rate $\dot{\psi}_c$ and the zero lateral load factor n_y. The FDI system indicates to the MPC lateral controller which actuator has failed and at which commanded deflection.

During the flight experiment, the crew had authority to select both airspeed and altitude through the guidance panel situated in the cockpit. The sequence of waypoints was defined before flight and incorporated into the Simulink® model.

A. Controller Design

The fault-tolerant lateral autopilot was constructed considering an ATTAS linear model obtained with calibrated airspeed $V_{\text{CAS}}=$ 160 kt, pressure altitude of 12,000 ft, and gear and flaps up. The lateral state vector is

$$x = [\,p \quad r \quad \phi \quad v_b \quad \delta_{a_r} \quad \delta_{a_l} \quad \delta_r\,]^T \tag{54}$$

where p is the roll rate (rad/s), $r \cong \dot{\psi}$ is the yaw rate (rad/s), ϕ is the bank angle (rad), v_b is the lateral velocity component in the body-fixed y axis (m/s), δ_{a_r} and δ_{a_l} are the right and left aileron deflections (rad), respectively, and δ_r is the rudder deflection (rad). The control

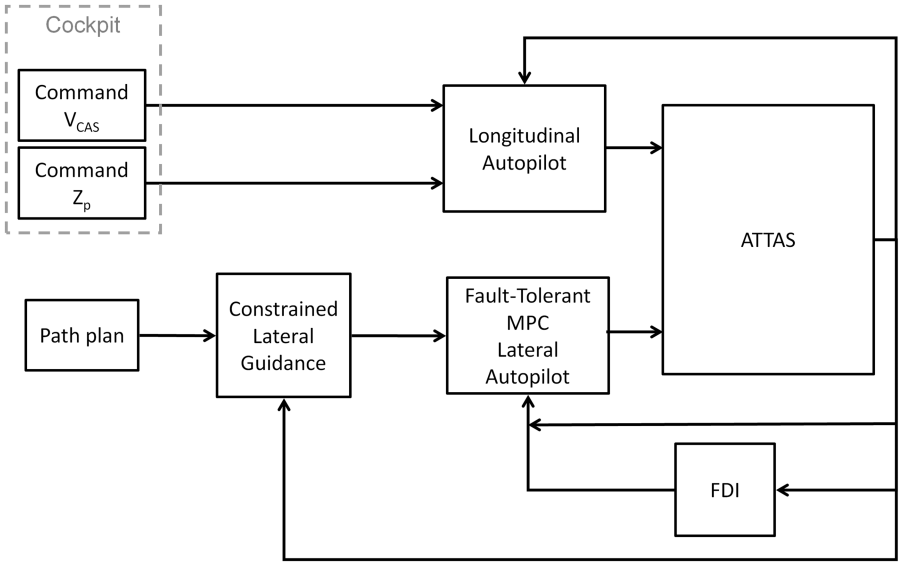

Fig. 8 Trajectory control system architecture.

vector is $u = [\delta_{a_c} \quad \delta_{r_c}]^T$, which represents the aileron command (rad) and the rudder command (rad). The asymmetrical power lever angle was not considered in this design, because of the presence of strong nonlinearities in the fuel control unit of the engines [41].

The performance output expressed by Eq. (1) is defined by $w_m = [p \quad r \quad \phi \quad v_b]^T$, that is required to follow the transient behavior specified by the model

$$A_m = \begin{bmatrix} -2.96 & 1.29 & -2.88 & -0.0274 \\ -0.133 & -1.44 & -0.109 & 0.0226 \\ 1 & 0.0825 & 0 & 0 \\ 7.86 & -93.3 & 9.54 & -0.168 \end{bmatrix} \tag{55}$$

The weight matrices Q and R of Eq. (6) were set as $Q = 100I$ and $R = 1 \times 10^{-10} I$. The discretization of the dynamical system and the weight matrices has been done with $T_s = 0.05$ s, from which the matrices Φ, Γ, Q_d, W_d, and R_d are obtained, as well as the feedback gain K_d:

$$K_d = \begin{bmatrix} -0.952 & -0.583 & -2.19 & 0.00206 & 0.901 & 0.891 & -0.00537 \\ 0.348 & -3.2 & 0.227 & 0.00486 & -0.00264 & -0.00264 & 1.72 \end{bmatrix} \tag{56}$$

Several control horizons were investigated in the ground simulator before the flight test. Small values of N provided faster constrained control computation, but with abrupt control variations. Increasing the control horizon tends to smooth the solution [27]. Therefore larger values of N were implemented and tested until full utilization was made of the available onboard computational power, which was also shared with several functionalities of the complete trajectory-tracking system. Hence, a value of $N = 20$ was selected for the MPC regulator.

The target calculation problem assumes that the controlled variables are $z = [\dot{\psi} \quad n_y]^T$ and also that the full state is observed, which leads, with respect to Eq. (19), to $E = I$ and

$$H = \begin{bmatrix} 0 & 1 & 0 & 0 & 0 & 0 & 0 \\ 0.0166 & 0.0964 & 0 & -0.0164 & 0 & 0 & 0.293 \end{bmatrix} \tag{57}$$

The constrained target calculator comprises another quadratic programming problem. However, in this experiment, some priority has been given to the investigation of the constrained regulator with implicit model following, which demanded considerable computational power. Therefore, an unconstrained target calculation has been chosen to compute the state x_{ss} and control vector u_{ss}. This is done with the solution of Eq. (23) expressed by

$$\begin{bmatrix} x_{ss} \\ u_{ss} \end{bmatrix} = \begin{bmatrix} X_r \\ U_r \end{bmatrix} r_{ss} \tag{58}$$

because the disturbance model was not taken into consideration in this experiment. The impact of this simplification is the possible presence of tracking errors during steady state, when the aircraft moves from the nominal condition. In this case, the closed-loop stability is guaranteed within a certain operating range due to the stabilizing properties of the constrained regulator.

For the considered flight condition and controlled variables, the matrices of Eq. (58) are given by

$$X_r = \begin{bmatrix} -0.0825 & 0 \\ 1 & 0 \\ 10 & -1 \\ -0.319 & -89.5 \\ 0.137 & 0.156 \\ 0.141 & 0.16 \\ -0.343 & -1.6 \end{bmatrix}, \qquad U_r = \begin{bmatrix} 0.188 & 0.215 \\ -0.439 & -2.04 \end{bmatrix} \tag{59}$$

The admissible sets related to the reconfigurable control problem must be established. In the nominal conditions (i.e., without faults in the actuators), the sets of admissible controls were defined as

$$-15^\circ \le \delta_{a_c} \le 15^\circ \qquad -10^\circ \le \delta_{r_c} \le 10^\circ \tag{60}$$

The terminal constraint $x_N \in O_\infty$, established in the problem Eq. (18), is relaxed in this experiment, because terminal constraints introduce additional complexity in the quadratic programming problem, and, subsequently, extra computational burden, compromising the capability of the onboard experimental computer to calculate an optimal control action within the tight sampling time.

The lateral deviation of the aircraft to the active leg of navigation was computed considering the last waypoint as the origin of the local reference system [41]. Moreover, because the airspeed changes during the flight, a gain scheduling has been implemented into the constrained guidance system with different gains K_g and related gains of transition, as function of calibrated airspeed V_{CAS}. Hence, Eq. (45) turns into a more general form:

$$\mathrm{DTA} = \lambda(V_{\mathrm{CAS}}) \frac{\Delta\chi_T}{\sin(\Delta\chi_T)} \tag{61}$$

B. Simulated Aileron Fault

During the flight test, a simulated aileron fault was injected through reducing its maximum displacement to $\pm 0.8^\circ$. This modification was done online by simply replacing the constraints of the quadratic programming with constraints of small aileron displacement. The consequence of a faulty aileron is the reduction of the maximum statically commandable turn rate to the autopilot. Once the target control is calculated by Eq. (58), the new limits of turn rate are directly obtained by substitution, leading to $\dot{\psi}_{c_{\min}} = -\dot{\psi}_{c_{\max}} = 4.25^\circ/\mathrm{s}$ with zero command of lateral load factor.

It is worth mentioning the performance limitations of the proposed transition logic. For a maximum commanded turn rate to the autopilot, there is a maximum allowable $\Delta\chi_T$. Sharper transitions will need larger turn rates, more than feasible by the fault-tolerant

Table 1 Planned trajectory for ATTAS flight test

Waypoint	Latitude, deg	Longitude, deg	V_{CAS} run 1	V_{CAS} run 2
1	52.1890	10.7889	160	190
2	52.2473	10.5455	160	170
3	52.3867	10.5251	160	160
4	52.4903	10.6030	160	——
5	52.5361	10.8089	160	——
6	52.4817	11.0245	160	——
7	52.3564	11.0688	180	——
8	52.2358	10.9988	180	——

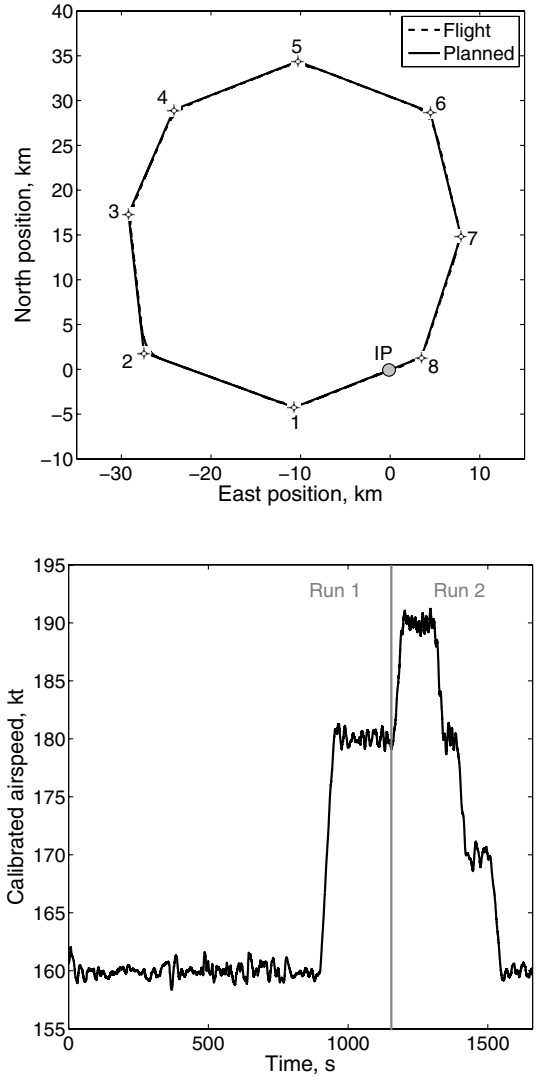

Fig. 9 Navigation horizontal view and calibrated airspeed.

autopilot. Because the limitation of the autopilot is $\dot{\psi}_{c_{\max}} = -\dot{\psi}_{c_{\min}} = 4.25°/\text{s}$ with a faulty aileron, the maximum $\Delta\chi_T$ is equal to 2.26 rad (=129.4°). Therefore, the effects of an actuator fault are communicated to the path-planning level, imposing restrictions on the distribution of the waypoints.

Table 2 Maximum predicted and in-flight yaw rates with $V_{\text{CAS}} = 160$ kt

Waypoint	$\Delta\chi_T$, deg	Max. predicted $\dot{\psi}$, deg/s	Max. in-flight $\dot{\psi}$, deg/s
1	41.3	1.36	1.24
2	63.5	2.09	2.03
3	29.7	0.98	1.03
4	45.3	1.49	1.72
5	42.5	1.40	1.75
6	55.4	1.82	2.18

C. Experimental Setup

The proposed system was implemented in Simulink environment. The MPC constrained optimization problem was solved through a quadratic programming solver. The active set method of Goldfarb and Idnani [42] was converted into an S-function, which could be compiled for several target environments. After that, an executable file was built, using Real-Time Workshop®, which could be tested using the ATTAS ground-based simulator. Several simulations have been performed, considering various scenarios of wind, aircraft initial position, demanded vertical profiles, and control horizons N. The ATTAS flight-test crew evaluated the proposed controller under those scenarios to give final acceptance. Once approved, the controller was patched and boarded inside the experimental computer of the ATTAS test vehicle. Detailed descriptions of this procedure and the interface of the experimental computer with the flight control system are given by Gestwa et al. [43].

D. Experimental Results

The flight test on the ATTAS vehicle was executed in July 2008 using the Braunschweig airfield for takeoff and landing operations. A trajectory defined by geodetic waypoints and target airspeeds was planned according to Table 1; this trajectory attempted to respect the maximum admissible angle between legs in the faulty condition. The altitude was held constant at FL120. The experimental computer engagement was done in the navigation leg defined by waypoints 8 and 1. After passing by waypoint 1, the simulated aileron fault was injected. Two consecutive runs were executed to allow transitions with different airspeeds.

Figure 9 shows the executed horizontal profile and evolution of calibrated airspeed during the two runs. The initial position has horizontal Cartesian coordinates (0, 0). The lateral guidance and control system shows adequate tracking performance, even in the presence of considerable winds, about 20–25 kt from the west direction. The transitions were executed correctly and no lateral overshoot was observed. The transitions of waypoints 1 and 2 were

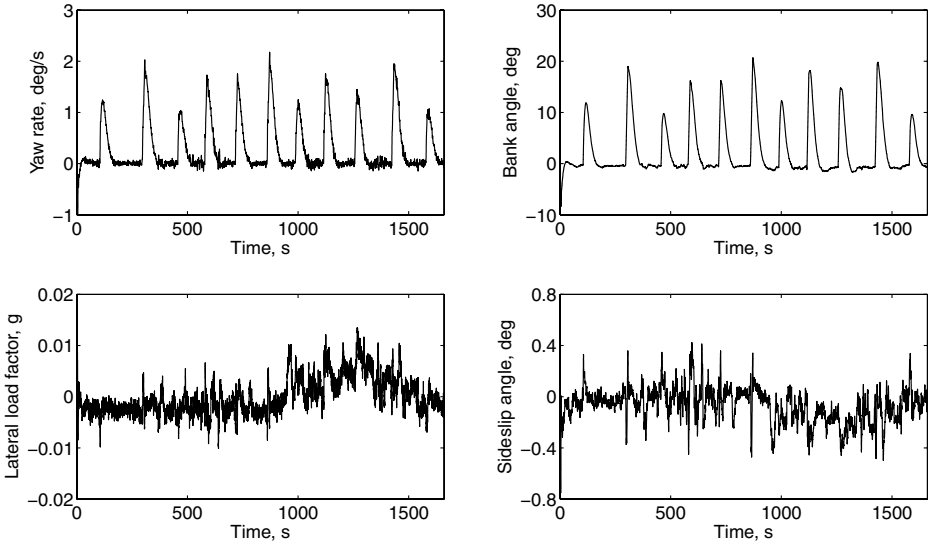

Fig. 10 Evolution of aircraft dynamical variables.

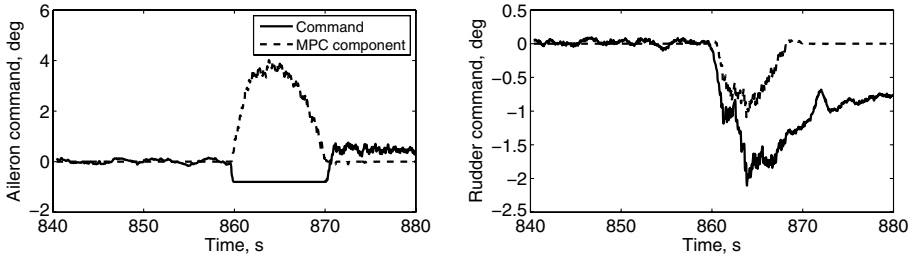

Fig. 11 Evolution of aileron and rudder commands during transition of waypoint 6.

executed twice, with different airspeeds, and the resulting trajectories were almost identical.

Figure 10 presents the evolution of relevant dynamical variables. One of the effects of airspeed change can be seen in the time history of the lateral load factor. The autopilot has been designed to track load factor in the nominal condition with $V_{\text{trim}} = 97.8$ m/s. Therefore, moving from the trimmed condition would generate some steady-state errors, as was observed after 1000 s of experiment. The small error in lateral load factor came with an angle of sideslip offset. However, this small acceleration was not noticed by either the cabin crew or the experimental crew. The yaw rate response was maintained inside the admissible autopilot demand set because the waypoints had been distributed to respect the maximum transition angle. Moreover, the maximum achieved values maintained adequate correlation with the predicted values, as shown by Table 2.

After the fault simulation, the aileron command deflection has respected the limitation of $\pm 0.8°$, as shown during the transition of waypoint 6 in Fig. 11. Also, the contribution of the MPC component can be seen, which reduces the value of the unconstrained LQR solution to keep the command inside the admissible set. The correction component of the rudder command worked to maintain the response closer to the nominal model, adding more deflection to the unconstrained solution. The desired reconfigurability of the proposed autopilot was demonstrated by both MPC components, because they were maintained at zero, unless some input reached its saturation value.

VI. Conclusions

A new form of fault-tolerant flight control system based on model predictive control is presented in this work. The proposed solution has the ability to redistribute control effort among the aerodynamic surfaces and engines after the occurrence of a fault, to track a certain reference value and to maintain the nominal closed-loop transient behavior. Thus, the fault-tolerant technique is suitable for applications in the inner-loop, such as lateral and longitudinal autopilots.

The design of the fault-tolerant controller must take into consideration the fact that certain control resources, which are not required during normal operation, become essential in abnormal conditions. This capability is illustrated by the simulation results of a lateral autopilot. During normal operation, asymmetrical usage of the engines is not necessary but it appears automatically in a faulty scenario (e.g., compensating for the effects of a jammed rudder).

Another important result is the proposal of a lateral guidance system that smooths the path when the aircraft is passing by a specific waypoint. Also, the guidance control law calculates the constrained and low-bandwidth demands to the lateral autopilot, which could present reduced dynamical performance after the occurrence of an actuator or a structural fault.

A complete trajectory-tracking control system that was composed of the fault-tolerant controller and the new lateral guidance system has been successfully tested in-flight. The flight control system computer had sufficient processing power to conduct constrained optimization of the model predictive controller at each sampling time, as well as guidance and navigation calculations.

Acknowledgments

This research was supported by the DLR, German Aerospace Center and by the Grupo Especial de Ensaios em Vôo do Departamento de Ciência e Tecnologia Aeroespacial (GEEV-DCTA) under doctoral project number 547. Fabio A. de Almeida has carried out this work during tenure at Institute of Flight Systems, DLR.

References

[1] Osder, S., "Practical View of Redundancy Management—Application and Theory," *Journal of Guidance, Control, and Dynamics*, Vol. 22, No. 1, Jan.–Feb. 1999, pp. 12–21. doi:10.2514/2.4363

[2] Briere, D., and Traverse, P., "AIRBUS A320/A330/A340 Electrical Flight Controls—A Family of Fault-Tolerant Systems," *Proceedings of the 23rd International Symposium on Fault-Tolerant Computing*, Inst. of Electrical and Electronics Engineers, Piscataway, NJ, June 1993, pp. 616–623.

[3] Jategaonkar, R., *Flight Vehicle System Identification: A Time Domain Methodology*, 1st ed., AIAA, Reston, VA, 2006, Chap. 1.

[4] Heise, S., and Maciejowski, J., "Model Predictive Control of a Supermaneuverable Aircraft," AIAA Guidance, Navigation, and Control Conference, AIAA Paper 1996-3768, San Diego, CA, July 1996.

[5] Maciejowski, J., and Jones, C., "MPC Fault-Tolerant Flight Control Case Study: Flight 1862," *Proceedings of the IFAC SAFEPROCESS 2003*, International Federation of Automatic Control, Laxenburg, Austria, June 2003, pp. 119–124.

[6] Kale, M., and Chipperfield, A., "Reconfigurable Flight Control Strategies Using Model Predictive Control," *Proceedings of the IEEE International Symposium on Intelligent Control*, Inst. of Electrical and Electronics Engineers, Piscataway, NJ, Oct. 2002, pp. 43–48.

[7] Kale, M., and Chipperfield, A., "Robust and Stabilized MPC Formulations for Fault Tolerant and Reconfigurable Flight Control," *Proceedings of the IEEE International Symposium on Intelligent Control*, Inst. of Electrical and Electronics Engineers, Piscataway, NJ, Sept. 2004, pp. 222–227.

[8] Luo, Y., Serrani, A., Yurkovich, S., Doman, D., and Oppenheimer, M., "Model Predictive Dynamic Control Allocation with Actuator Dynamics," *Proceedings of the 2004 American Control Conference*, Vol. 2, Inst. of Electrical and Electronics Engineers, Piscataway, NJ, June 2004, pp. 1695–1700.

[9] Luo, Y., Serrani, A., Yurkovich, S., Oppenheimer, M. W., and Doman, D. B., "Model-Predictive Dynamic Control Allocation Scheme for Reentry Vehicles," *Journal of Guidance, Control, and Dynamics*, Vol. 30, No. 1, Jan.–Feb. 2007, pp. 100–113. doi:10.2514/1.25473

[10] Mayne, D., Rawlings, J., Rao, C., and Scokaert, P., "Constrained Model Predictive Control: Stability and Optimality," *Automatica*, Vol. 36, No. 6, 2000, pp. 789–814. doi:10.1016/S0005-1098(99)00214-9

[11] Muske, K., and Rawlings, J., "Model Predictive Control with Linear Models," *AIChE Journal*, Vol. 39, No. 2, 1993, pp. 262–287. doi:10.1002/aic.690390208

[12] Blanchini, F., "Set Invariance in Control," *Automatica*, Vol. 35, No. 11, 1999, pp. 1747–1767. doi:10.1016/S0005-1098(99)00113-2

[13] Maeder, U., and Morari, M., "Offset-Free Reference Tracking for Predictive Controllers," *Proceedings of the 46th IEEE Conference on Decision and Control*, Inst. of Electrical and Electronics Engineers, Piscataway, NJ, Dec. 2007, pp. 5252–5257.

[14] Maciejowski, J. M., "The Implicit Daisy-Chaining Property of Constrained Predictive Control," *Applied Mathematics and Computer Science*, Vol. 8, No. 4, 1998, pp. 695–712.

[15] Strube, M., Sanner, R., and Atkins, E., "Dynamic Flight Guidance Recalibration After Actuator Failures," *1st AIAA Intelligent Systems Technical Conference*, AIAA Paper 2004-6255, Chicago, IL, Sept. 2004.

[16] Schierman, J., Ward, D., Hull, J., and Gandhi, N., "Integrated Adaptive

Guidance and Control for Re-Entry Vehicles with Flight-Test Results," *Journal of Guidance, Control, and Dynamics*, Vol. 27, No. 6, Nov.–Dec. 2004, pp. 975–985.
doi:10.2514/1.10344

[17] Atkins, E., Portillo, I., and Strube, M., "Emergency Flight Planning Applied to Total Loss of Thrust," *Journal of Aircraft*, Vol. 43, No. 4, July–Aug. 2006, pp. 1205–1216.
doi:10.2514/1.18816

[18] Ducard, G., Kulling, K., and Geering, H., "Evaluation of Reduction in the Performance of a Small UAV After an Aileron Failure for an Adaptive Guidance System," *Proceedings of the 2007 American Control Conference*, Inst. of Electrical and Electronics Engineers, Piscataway, NJ, July 2007, pp. 1793–1798.

[19] Kreindler, E., and Rothschild, D., "Model-Following in Linear-Quadratic Optimization," *AIAA Journal*, Vol. 14, No. 7, 1976, pp. 835–842.
doi:10.2514/3.7160

[20] Stengel, R., and Huang, C., "Restructurable Control Using Proportional-Integral Implicit Model Following," *Journal of Guidance, Control, and Dynamics*, Vol. 13, No. 2, 1990, pp. 303–309.
doi:10.2514/3.20550

[21] Patton, R., "Fault-Tolerant Control: the 1997 Situation," *Proceedings of the IFAC SAFEPROCESS 1997*, Vol. 3, International Federation of Automatic Control, Laxenburg, Austria, 1997, pp. 1033–1054.

[22] "Flying Qualities of Piloted Aircraft," U.S. Dept. of Defense, MIL-STD-1797A, Jan. 1990.

[23] Tomczyk, A., "Handling Qualities Augmentation System for General Aviation Aircraft," AIAA Guidance, Navigation, and Control Conference and Exhibit, AIAA Paper 2001-4264, Montreal, Aug. 2001.

[24] Ren, W., and Beard, R., "Trajectory Tracking for Unmanned Air Vehicles with Velocity and Heading Rate Constraint," *IEEE Transactions on Control Systems Technology*, Vol. 12, No. 5, 2004, pp. 706–716.
doi:10.1109/TCST.2004.826956

[25] Bryson, A., *Control of Spacecraft and Aircraft*, Princeton Univ. Press, Princeton, NJ, 1994, Appendix D.

[26] Loan, C., "Computing Integrals Involving the Matrix Exponential," *IEEE Transactions on Automatic Control*, Vol. 23, No. 3, 1978, pp. 395–404.
doi:10.1109/TAC.1978.1101743

[27] Rossiter, J., Kouvaritakis, B., and Rice, M., "A Numerically Robust State-Space Approach to Stable-Predictive Control Strategies," *Automatica*, Vol. 34, No. 1, 1998, pp. 65–73.
doi:10.1016/S0005-1098(97)00171-4

[28] Maciejowski, J. M., *Predictive Control with Constraints*, Prentice–Hall, Upper Saddle River, NJ, 2002, Chap. 3.

[29] Kwakernaak, H., and Sivan, R., *Linear Optimal Control Systems*, Wiley-Interscience, New York, 1972, pp. 270–272.

[30] Skogestad, S., and Postlethwaite, I., *Multivariable Feedback Control—Analysis and Design*, 2nd ed., Wiley, Hoboken, NJ, 2005, Chap. 9.

[31] Francis, B., and Wonham, W., "The Internal Model Principle of Control Theory," *Automatica*, Vol. 12, No. 5, 1976, pp. 457–465.
doi:10.1016/0005-1098(76)90006-6

[32] Pannocchia, G., Laachi, N., and Rawlings, J., "A Candidate to Replace PID Control: SISO-Constrained LQ Control," *AIChE Journal*, Vol. 51, No. 4, 2005, pp. 1178–1189.
doi:10.1002/aic.10373

[33] Pannocchia, G., and Kerrigan, E., "Offset-Free Receding Horizon Control of Constrained Linear Systems," *AIChE Journal*, Vol. 51, No. 12, 2005, pp. 3134–3146.
doi:10.1002/aic.10626

[34] Pannocchia, G., and Rawlings, J., "Disturbance Models for Offset-Free Model-Predictive Control," *AIChE Journal*, Vol. 49, No. 2, 2003, pp. 426–437.
doi:10.1002/aic.690490213

[35] Stengel, R. F., *Flight Dynamics*, Princeton Univ. Press, Princeton, NJ, 2004, Chap. 4.

[36] Rao, C., and Rawlings, J., "Steady States and Constraints in Model Predictive Control," *AIChE Journal*, Vol. 45, No. 6, 1999, pp. 1266–1278.
doi:10.1002/aic.690450612

[37] Whang, I., and Hwang, T., "Horizontal Waypoint Guidance Design Using Optimal Control," *IEEE Transactions on Aerospace and Electronic Systems*, Vol. 38, No. 3, 2002, pp. 1116–1120.
doi:10.1109/TAES.2002.1039430

[38] Kvasnica, M., Grieder, P., Baotic, M., and Morari, M., "Multi-Parametric Toolbox (MPT)," *Hybrid Systems: Computation and Control*, Springer-Verlag, New York, April 2004, pp. 448–462.

[39] Gilbert, E., and Tan, K., "Linear Systems with State and Control Constraints: The Theory and Application of Maximal Output Admissible Sets," *IEEE Transactions on Automatic Control*, Vol. 36, No. 9, 1991, pp. 1008–1020.
doi:10.1109/9.83532

[40] Stevens, B. L., and Lewis, F. L., *Aircraft Control and Simulation*, 2nd ed., Wiley, Hoboken, NJ, 2003, Chap. 4.

[41] Almeida, F., "Waypoint Navigation Using Constrained Infinite Horizon Model Predictive Control," AIAA Guidance, Navigation, and Control Conference and Exhibit, AIAA Paper 2008-6462, Honolulu, HI, Aug. 2008.

[42] Goldfarb, D., and Idnani, A., "A Numerically Stable Dual Method for Solving Strictly Convex Quadratic Programs," *Mathematical Programming*, Vol. 27, No. 1, Sept. 1983, pp. 1–33.
doi:10.1007/BF02591962

[43] Gestwa, M., Leißling, D., and Bauschat, J., "The Software Development Environment of the Flying Test-Bed ATTAS," AIAA Modeling and Simulation Technologies Conference and Exhibit, AIAA Paper 2005-6211, San Francisco, Aug. 2005.